

# Fluidization of Wet Granulates under Hydrodynamic Shear

I. BATTIATO AND J. VOLLMER

Max Planck Institute for Dynamics and Self-Organization, 37073 Göttingen, Germany, EU

(Received ?? and in revised form ??)

We investigate the fluidization threshold of three-dimensional cohesive granulates under hydrodynamic shear forces exerted by a creeping flow. A continuum model of flow through porous media provides an analytical expression for the average drag force on a single grain. The balance equation for the forces and a force propagation model are then used to investigate the effects of porosity and packing structure on the stability of the pile. We obtain a closed-form expression for the fluidization threshold of a regular packing of mono-disperse frictionless cohesive spherical grains in a planar fracture. The compound effect of structural (packing orientation and porosity) and dynamical properties of the system on its stability is quantified.

**Key Words:** Fluidization threshold, wet granulate, Brinkman equation, force network model, multiscale model, hydrodynamic force, instability

## 1. Introduction

Granulates are a large collection of macroscopic solid grains. Dry and wet granulates are vital in a large variety of industries, ranging from pharmaceutical to mining (Duran 2000, pp. 4-10), from construction to agricultural (Duran 2000, pp. 10). They also play an important role in many geological processes (Duran 2000, par. 1.3), such as land and mudslides (Dikau & Brunsden 1996), debris flows (Iverson *et al.* 2000), erosion, dune formation (Bagnold 1941), that shape planets' morphology including, but not limited to, Earth (Hansen *et al.* 2011). Despite their ubiquity in natural systems, granular materials and their behaviour have received considerable attention in the physics community only in the last two decades due to their peculiar properties, very different from those commonly associated with either solids, liquids, or gases (Jaeger, Nagel & Behringer 1996; Hornbaker *et al.* 1997; Schiffer 2005; Novak, Samadani & Kudrolli 2005, and references therein).

Most theoretical and experimental studies focus on dry granulates and their collective behaviour including pattern formation (e.g., Umbanhowar, Melo & Swinney 1996; Hansen *et al.* 2011), angle of stability/repose (e.g., Jaeger, Liu & Nagel 1989; Alonso & Herrmann 1996), avalanches dynamics (e.g., Jop, Forterre & Pouliquen 2006, 2007) and granular flows (e.g., Rajchenbach 2003; MiDi 2004).

However, as every child knows, adding even a small quantity of liquid to a sandpile dramatically changes its properties. The cohesion between grains, due to capillary forces, greatly enhances the stability of wet samples. The collective behaviour of wet grains has only recently begun to be explored (Jaeger, Nagel & Behringer 1996; Herminghaus 2005, and references therein). The effects of humidity and capillary attractive forces due to liquid bridges has a huge impact for practical applications as grains are often not dry

in many industrial processes, e.g. when granulates are stored in open air and atmospheric humidity plays a role (Fray & Marone 2002), and natural systems, e.g. soil (Iverson 2000). A number of studies have focused on the dynamics of wet granular avalanches (e.g., Tegzes, Vicsek & Schiffer 2003) and on the effect of humidity (Fraysse, Thomé & Petit 1999; Fray & Marone 2002; Restagno *et al.* 2002) and capillary forces (Albert *et al.* 1997; Hornbaker *et al.* 1997; Restagno, Bouquet & Charlaix 2004; Novak, Samadani & Kudrolli 2005) on the static properties of granulates. A number of different models have been proposed to study the geometric stability of wet piles, including Mohr-Coulomb continuum (Mason *et al.* 1999), liquid-bridge (Novak, Samadani & Kudrolli 2005) and response function (Ebrahimpour-Rahbari *et al.* 2009) models.

While invaluable in shedding light into the properties of wet granulates, natural systems often include a number of additional forcing factors that might significantly affect the stability of granulates in the environment. In geological systems, instability is triggered by a combination of body forces (e.g. gravity) and hydrodynamic shearing due to the creeping motion of a fluid through a (often saturated) cohesive granulate. This is especially true in processes such as cliffs' instability and landslides, where a fluidization event is triggered after heavy rainfall, sediment transport in submerged environments (e.g. seafloor transport), fluidization of fines in fractures during pumping operations or oil recovery, just to mention a few. Therefore, the understanding of how hydrodynamic forces affect the stability of granular matter is of utmost importance to better quantify the processes that trigger a fluidization event in submerged granular cohesive systems. Moreover, structural properties of cohesive piles, such as porosity, can have a dramatic impact on their stability (Iverson *et al.* 2000).

In the present work we use a multi-scale framework to quantify the effect of hydrodynamic forces on the onset of instability (i.e. fluidization) of a pile constituted of cohesive (e.g. oil-wet) grains in a planar fracture. On one hand, a continuum-scale model is used to calculate the average hydrodynamic drag exerted on the grains; on the other, a pore-scale network model allows us to calculate the force chains propagating through the pile and to analytically identify the location of failure and the fluidization threshold of regular packing structures for mono-disperse frictionless spherical grains. These are determined as a function of structural (e.g. porosity, grain contacts distribution) and dynamical (e.g. capillary and hydrodynamic forces) properties of the system. For simplicity, gravity is here neglected. Generalisation to include gravity effects is straightforward.

In section 2 we introduce a continuum-scale Darcy-Brinkmann model for the flow and the hydrodynamic force exerted from the creeping fluid on the granulate (Battiato, Bandaru & Tartakovsky 2010; Battiato 2011). Such model treats the wet granulate as porous medium. Therefore, the average drag force exerted on each layer of the pile can be calculated from continuum-scale equations. Section 3 discusses a pore-scale network model for the force propagation through the pile. Location of failure, maximum load and fluidization threshold are analytically derived. Finally, the stability criterion is formulated in terms of the capillary number, that represents the relative strength between destabilising hydrodynamic shear and stabilising capillary (cohesive) forces, and the packing orientation relative to the average flow direction. The main results and conclusions are summarised in section 4.

## 2. Continuum-scale Model of Flow and Drag

We consider a fully developed incompressible fluid flow between two infinite parallel plates separated by the distance of  $H + 2L$  (Fig. 1). The bottom part of the flow domain,  $-H < \hat{y} < 0$ , is occupied by a regular packing of (oil-) wet mono-disperse rigid frictionless

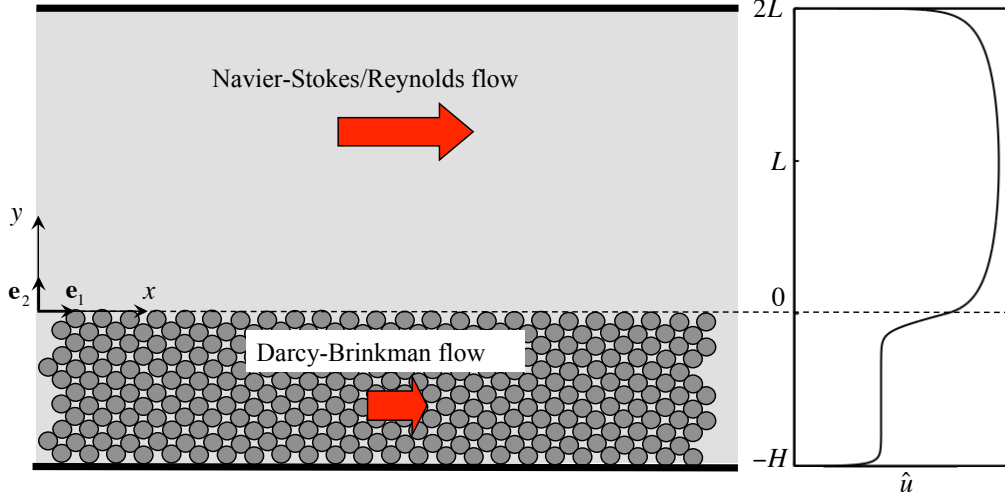


FIGURE 1. Schematic of the domain on the right, and shape of the average velocity profile through the channel, on the left.

spheres of radius  $R$ . The flow is driven by an externally imposed (mean) constant pressure gradient  $d\hat{p}/d\hat{x} < 0$ . Therefore, each spherical grain is subject to a drag force due to hydrodynamic stresses and attractive capillary bridge forces. We determine the stability regime of this wet three-dimensional sphere packing as a function of hydrodynamic drag and packing orientation and structure.

### 2.1. Geometry and Packing

In the present work, we focus on three-dimensional isostatic mono-disperse sphere packing obtained by expanding a cubic centred close packing, CCP, so to eliminate interlayer contacts. Such expanded packing configuration will be referred to as CEP (Cubic-Expanded-Packing). Figures 2(a) and (b) show the side and top view of the structure of the first two layers (AB) of spheres. Figure 2(c) shows the top view of a full CEP structure.

Let us consider a regular pile of two layers of mono-disperse spheres with radius  $R$ . Let  $\hat{\ell}$ ,  $2R < \hat{\ell} < 2\sqrt{3}R$ , be the pitch in the  $x - z$  (horizontal) plane, i.e. the distance between the centers of spheres belonging to the same layer, and  $\hat{h}$  the pitch in the  $y - z$  (vertical) plane, i.e. the distance between two adjacent layers (Fig. 2). When  $\hat{\ell} = 2R$ ,  $\hat{h} = 2\sqrt{6}R/3$ , the regular close packing is recovered (CCP) and the structure obtained by connecting the centers of the four spheres corresponds to a regular tetrahedron (see Fig. 2(a)). If  $\hat{\ell} = 2\sqrt{3}R$ ,  $\hat{h} = 0$  and the four spheres lie on the same level.

Let us define dimensionless quantities

$$h = \frac{\hat{h}}{H}, \quad \ell = \frac{\hat{\ell}}{H}, \quad \epsilon = \frac{2R}{H}. \quad (2.1)$$

The dimensionless interlayer and intralayer distances  $h$  and  $\ell$  are related as follows

$$h = \epsilon \sqrt{1 - \frac{1}{3} \left( \frac{\ell}{\epsilon} \right)^2}, \quad \epsilon < \ell < \sqrt{3}\epsilon, \quad (2.2)$$

and the porosity  $\phi$  amounts to

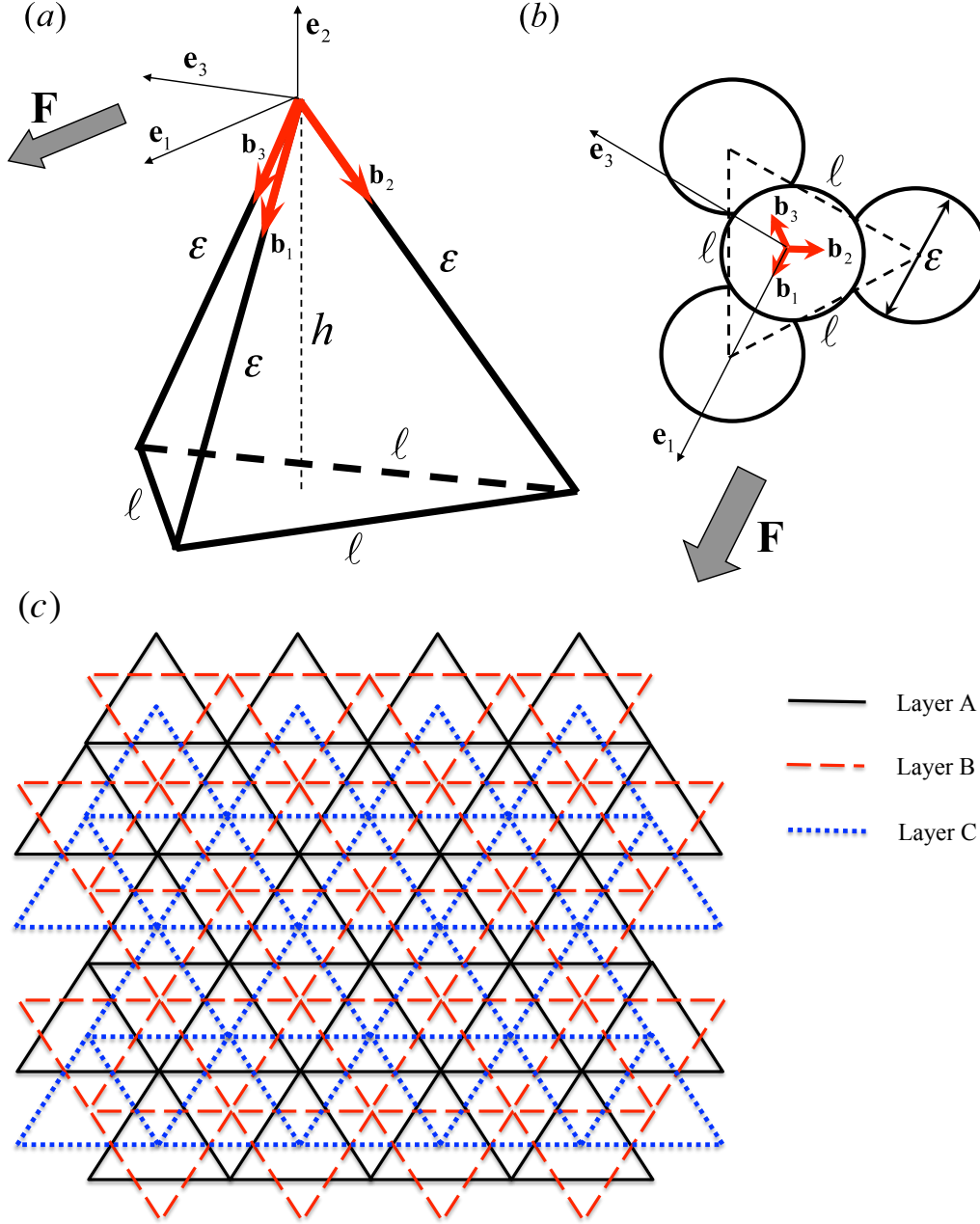


FIGURE 2. Side (a) and top view (b) of the structure of a two-layer 3-dimensional regular pile of spheres of diameter  $\epsilon$  and intralayer distance  $\epsilon < \ell < \sqrt{3}\epsilon$ . The distance between the centers of two adjacent layers of spheres is  $h$ . (c) Top view of a cubic stacking showing the connections between spheres' centers belonging to the same layer: from the first two layers of spheres (AB), a CEP arrangement can be obtained if every third layer (i.e. ABCABC...) is the same.

$$\phi = 1 - \pi \left[ 3 \left( \frac{\ell}{\epsilon} \right)^2 \sqrt{3 - \left( \frac{\ell}{\epsilon} \right)^2} \right]^{-1} \quad \epsilon < \ell < \sqrt{3}\epsilon. \quad (2.3)$$

When  $\ell = \epsilon$  the close packing is recovered and  $\phi \rightarrow \phi_c \approx 0.26$ , corresponding to a closed packing fraction of spheres  $s_c = \pi/3\sqrt{2} \approx 0.74$ .

Let  $N + 1$  be the total number of layers in the pile and  $n = \{1, \dots, N\}$  denote the layer number. The bottom layer of grains, sitting on the channel's lower boundary, is immobile and is called a *wall*. The layer sitting immediately on the *wall* has  $n = 1$ . The layer enumeration continues moving up to the top-most layer in the pile where  $n = N$ . The number of mobile layers,  $N$ , and the height of the pile,  $H$ , are related through  $H = N\hat{h} + 2R$  or in terms of dimensionless quantities

$$N = \frac{1 - \epsilon}{h}. \quad (2.4)$$

The (continuum-scale) limit  $\epsilon \rightarrow 0$  corresponds to  $N(\epsilon) \approx (1/\epsilon - 1)/\sqrt{1 - (\ell/\epsilon)^2/3} \rightarrow \infty$  where  $\ell/\epsilon \in (1, \sqrt{3})$ .

## 2.2. Fluid flow model

Following (Battiato, Bandaru & Tartakovsky 2010; Battiato 2011), we treat the sphere-packed region, i.e. the region occupied by spheres, as a porous medium with porosity  $\phi$  and permeability  $K$ . A number of formulas are available to relate permeability to porosity for both dilute and non-dilute systems of mono-disperse spheres. In the dilute limit where velocity fields of the spheres do not interfere with each other, the permeability is given by the well-known Stokes result

$$k_s = \frac{2R^2}{9(1 - \phi)} \quad (2.5)$$

(Torquato 2000, pp.505, eq. (19.103)). For nondilute concentration of spheres, Howells (1974) and Hinch (1977) found

$$K = k_s \left[ 1 + \frac{3}{\sqrt{2}}(1 - \phi)^{1/2} + \frac{135}{64}(1 - \phi) \ln(1 - \phi) + 16.456(1 - \phi) + o(1 - \phi) \right]^{-1} \quad (2.6)$$

(Torquato 2000, p.508, eq. (19.119)). The flow in this region,  $\hat{y} \in (-H, 0)$ , can be described by the Brinkman equation for the horizontal component of the intrinsic average velocity  $\hat{u}$  (Auriault 2009),

$$\mu_e \frac{d^2 \hat{u}}{d\hat{y}^2} - \frac{\mu}{K} \hat{u} - \frac{d\hat{p}}{d\hat{x}} = 0, \quad \hat{y} \in (-H, 0), \quad (2.7)$$

where  $d\hat{p}/d\hat{x}$  is a mean constant pressure gradient,  $\mu$  is the fluid's dynamic viscosity, and  $\mu_e$  is its "effective" viscosity that accounts for the slip at the spheres walls. Since we are concerned with the fluidization threshold of the sphere packing, initially at rest, permeability is constant until the fluidization threshold is reached. This allows us to decouple an analysis of the flow from that of the granulate dynamics. In the rest of the flow domain,  $\hat{y} = [-2L, 0]$ , we use either Navier-Stokes or Reynolds equations to describe fully developed flow respectively in either laminar ( $\gamma = 0$ ) or turbulent ( $\gamma = 1$ ) regimes (Pope 2000, Eq. 7.8),

$$\mu \frac{d^2 \hat{u}}{d\hat{y}^2} - \gamma \rho \frac{d\langle \hat{u}' \hat{v}' \rangle}{d\hat{y}} - \frac{d\hat{p}}{d\hat{x}} = 0, \quad \hat{y} \in (0, 2L), \quad (2.8)$$

where  $\rho$  is the fluid density, and  $\hat{u}(\hat{y})$  is the horizontal component of flow velocity  $\hat{\mathbf{u}}(\hat{u}, \hat{v})$ . In the laminar regime,  $\hat{u}$  is the actual velocity and  $\hat{v} \equiv 0$ . In the turbulent regime, the actual velocity is decomposed into a mean velocity  $\hat{\mathbf{u}}$  and velocity fluctuations  $\hat{u}'$  and  $\hat{v}'$  about their respective means.  $\langle \hat{u}'\hat{v}' \rangle$  denotes the Reynolds stress. Fully-developed turbulent channel flow has velocity statistics that depend on  $\hat{y}$  only.

In both flow regimes, the no-slip condition requires zero velocity at  $\hat{y} = -H$  and  $\hat{y} = 2L$ , and the continuity of velocity and shear stress is prescribed at the interface,  $\hat{y} = 0$ , between the free and filtration flows (Vafai & Kim 1990):

$$\hat{u}(-H) = 0, \quad \hat{u}(2L) = 0, \quad \hat{u}(0^-) = \hat{u}(0^+) = \hat{U}, \quad \mu_e \left( \frac{d\hat{u}}{d\hat{y}} \right)_{\hat{y}=0^-} = \mu \left( \frac{d\hat{u}}{d\hat{y}} \right)_{\hat{y}=0^+} \quad (2.9)$$

where  $\hat{U}$  is an unknown matching velocity at the interface between channel flow and porous medium.

Let us introduce a characteristic Darcy velocity  $q = -(H^2/\mu)d\hat{p}/d\hat{x}$  and define dimensionless quantities

$$u = \frac{\hat{u}}{q}, \quad y = \frac{\hat{y}}{H}, \quad \delta = \frac{L}{H}, \quad M = \frac{\mu_e}{\mu}, \quad Da = \frac{K}{H^2}, \quad Re_p = \frac{\rho H q}{\mu}, \quad (2.10)$$

where  $Da$  is the Darcy number (e.g., Niel, Junqueira & Lage 1996, Eq. 6) and  $Re_p$  is the Reynolds number for porous flow. Then the flow equations (2.7)–(2.9) can be rewritten in a dimensionless form

$$M \frac{d^2 u}{dy^2} - \frac{u}{Da} + 1 = 0, \quad y \in (-1, 0), \quad (2.11)$$

$$\frac{d^2 u}{dy^2} - \gamma Re_p \frac{d\langle u'v' \rangle}{dy} + 1 = 0, \quad y \in (0, 2\delta), \quad (2.12)$$

subject to the boundary conditions

$$u(-1) = 0, \quad u(2\delta) = 0, \quad u(0^-) = u(0^+) = U, \quad M \frac{du}{dy}(0^-) = \frac{du}{dy}(y = 0^+), \quad (2.13)$$

where  $U = \hat{U}/q$  is the unknown dimensionless flow velocity at the interface between the free and porous flows.

The dimensionless version of (2.6) allows one to express the Darcy number  $Da$  in terms of porosity  $\phi$  and the relative diameter of the spheres  $\epsilon$ ,

$$Da = \epsilon^2 f(\phi), \quad (2.14)$$

where

$$f(\phi) = \frac{1}{18(1-\phi)} \left[ 1 + \frac{3}{\sqrt{2}}(1-\phi)^{1/2} + \frac{135}{64}(1-\phi) \ln(1-\phi) + 16.456(1-\phi) + o(1-\phi) \right]^{-1}. \quad (2.15)$$

The limit of  $Da \rightarrow Da_c$  with  $\phi \rightarrow \phi_c$ ,  $Da_c \approx 1.08\epsilon^2$  and  $\epsilon < 1$  (i.e. more than one layer of spheres) corresponds to the diminishing flow through the granular pile due to decreasing permeability, i.e., due to very dense packing of spheres. In this limit, the Brinkman correction term  $M d^2 u / dy^2$  in (2.11) becomes negligible and (2.11) reduces to Darcy's law. The limit of  $Da \rightarrow \infty$  corresponds to free flow and (2.11) reduces to the Stokes equation. According to (2.14) and its graphical representation in Figure 3,  $Da \ll 1$  for  $\epsilon < 1$  regardless of the magnitude of  $\phi$ . This implies that crowding effects cannot be neglected for multiple layers of packed spheres. Even in high porosity packing

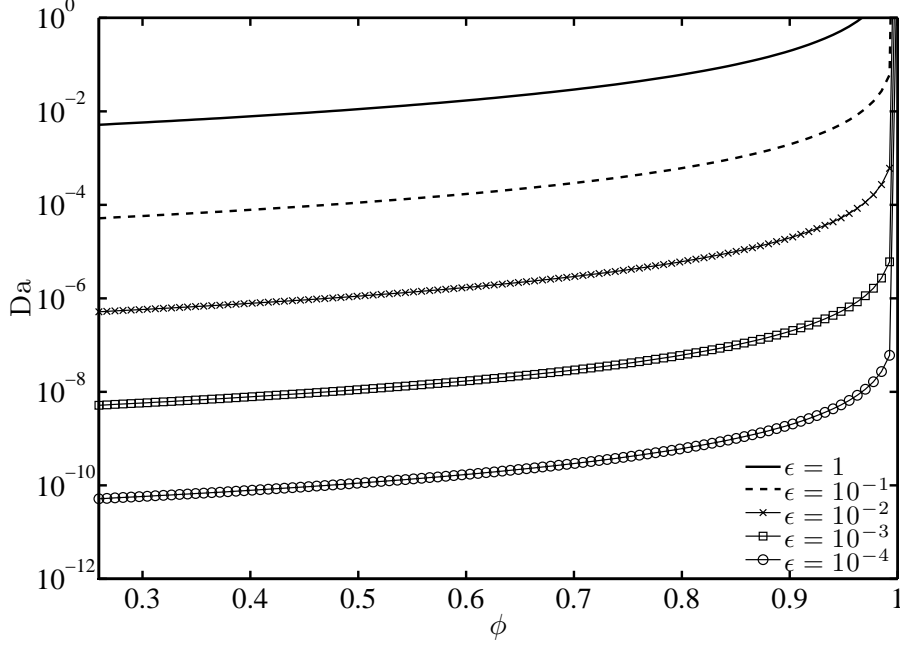


FIGURE 3. Darcy number  $Da$  as a function of porosity  $\phi$  and the aspect ratio  $\epsilon$  (Eq. (2.14)).

( $\phi \approx 0.8 - 0.9$ ), common values of  $\epsilon \approx 10^{-2} - 10^{-3}$  (e.g. fracture aperture of  $100\mu m$  and clay particle size less than  $2\mu m$ ) give rise to  $Da \approx 10^{-6} - 10^{-8}$ .

### 2.3. Hydrodynamic drag on spheres in non-uniform flow

The drag force per horizontal unit area exerted by the fluid on any cross-section  $y = \text{const}$  is given by the  $xy$ -component of the stress tensor  $\hat{\sigma}_{xy}(y)$ ,

$$\hat{\sigma}_{xy} = \alpha_\mu \frac{d\hat{u}}{d\hat{y}}, \quad (2.16)$$

where  $\alpha_\mu = \mu_e$  for  $\hat{y} \in [-H, 0]$ , and  $\alpha_\mu = \mu$  for  $\hat{y} \in [0, 2L]$ . The drag force distribution along the pile, i.e. the horizontal component of the force  $\hat{\mathbf{D}} = [\hat{\mathcal{D}}(\hat{y}), 0, 0]$ , is obtained as

$$\hat{\mathcal{D}} = \hat{\sigma}_{xy} / \hat{\mathcal{N}} = \mu_e \hat{\ell} \frac{d\hat{u}}{d\hat{y}}, \quad (2.17)$$

where  $\hat{\mathcal{N}} = 1/\hat{\ell}$  is the number of grains per unit length in the horizontal plane.

Rewriting (2.17) in terms of the dimensionless quantities (2.10) and introducing dimensionless shear  $\sigma_{xy}$ ,

$$\sigma_{xy} = \frac{\hat{\sigma}_{xy} H}{q\mu}, \quad (2.18)$$

the dimensionless drag  $\mathcal{D}$  is

$$\mathcal{D}(y) = \ell M \frac{du}{dy}. \quad (2.19)$$

The dimensionless drag force  $\mathbf{F}(n) = [F(n), 0, 0]$  exerted by the fluid on a sphere be-

longing to the  $n$ -th layer can be obtained by integrating  $\mathcal{D}(y)$  over the layer height  $h$ ,

$$F(1) = \int_{-1}^{-1+(3h+\epsilon)/2} \mathcal{D}(y) dy \quad (2.20a)$$

$$F(i) = \int_{-1+ih}^{-1+(i+1)h} \mathcal{D}(y) dy, \quad i = 2, \dots, N-1 \quad (2.20b)$$

$$F(N) = \int_{-1+Nh}^0 \mathcal{D}(y) dy. \quad (2.20c)$$

Combining (2.20) with (2.19),

$$F(1) = \ell M u(3h/2 + \epsilon/2 - 1) \quad (2.21a)$$

$$F(i) = \ell M [u(-1 + (i+1)h) - u(-1 + ih)], \quad i = 2, \dots, N-1 \quad (2.21b)$$

$$F(N) = \ell M [U - u(-1 + Nh)]. \quad (2.21c)$$

In the following section a pore-scale force network model is used to determine the location and the modulus of the maximum load in the pile from the hydrodynamic shear exerted by the fluid on each sphere.

### 3. Pore-scale Model of Failure

#### 3.1. Propagation of Forces

Let  $\mathbf{F}_k$  be the sum of the external forces acting on grain  $k$  (e.g. drag), and  $\mathbf{g}_{kl} = g_{kl}\mathbf{b}_{kl}$  the force exerted from grain  $k$  to grain  $l$ , where  $\mathbf{b}_{kl}$  is a unit vector pointing from grain  $k$  to grain  $l$  and  $g_{kl}$  is the magnitude of the force;  $g_{kl}$  is positive for compressive forces and negative otherwise. Whenever there is a stretched capillary bridge between two grains  $k$  and  $l$ , the force exerted by grain  $k$  on  $l$  is attractive and equal to a constant value  $\mathbf{f}_{kl} = f_b\mathbf{b}_{kl}$  where  $f_b > 0$ . This simplifying assumption that the capillary force is a constant, irrespective of grain separation distance, has demonstrated to provide good description of collective behaviour of wet granulates (Ebrahimpnazhad-Rahbari *et al.* 2009; Fingerle *et al.* 2008; Ulrich *et al.* 2009). The force distribution can be uniquely determined by solving the following system for the unknowns  $g_{kl}$

$$\sum_l \mathbf{g}_{kl} = \mathbf{F}_k, \quad \forall k, l = 1, \dots, M, \quad (3.1)$$

with  $M$  the total number of grains. There is a unique solution for the force distribution (Moukarzel 1998, 2004; Ebrahimpnazhad-Rahbari *et al.* 2009) in  $d$  dimensions, if the packing is isostatic, i.e., if the average number  $\nu$  of neighbours per grain equals  $2d$ . Note, however, that this solution does not necessarily comply with the constraint that contacts break when tensile forces exceed the capillary bridge force. Upon variation of parameters a packing yields when this additional requirement is first violated, i.e., the packing is stable as long as  $g_{kl} + f_b > 0$ ,  $\forall k, l$ .

In a regular isostatic 3-dimensional CEP packing of grains bounded by a solid wall at the bottom and a free surface at the top each sphere is supported by  $d = 3$  contacts from grains further down in the pile. For any couple  $(k, l)$  of grains in contact, the unit vector  $\mathbf{b}_{kl}$  connecting their centers is aligned to one of the (three) CEP-lattice directions. The external force exerted on each grain up in the pile propagates unchanged down through the pile to the first mobile layer ( $n=1$ ) along such directions as discussed in Ebrahimpnazhad-Rahbari *et al.* (2009). Therefore, the maximum load is experienced



from grains at the bottom of the pile, i.e.  $n = 1$ , and the stability threshold is determined by the respective bonds carrying the highest load.

Let  $\mathbf{F}$  be the maximum force exerted on each grain in the layer  $n = 1$  from the grains up in the pile. Let  $\mathbf{b}_\alpha$ ,  $\alpha = \{1, 2, 3\}$  be the unit vectors along the (lattice) directions connecting the center of the supported sphere in the first layer with the centers of the supporting spheres of the *wall* as shown in Fig. 4(a). The stabilizing capillary forces act along the directions  $\{\mathbf{b}_1, \mathbf{b}_2, \mathbf{b}_3\}$ . If the components of the total force  $\mathbf{F}$  along such directions are less than the capillary forces (assumed constant), the pile is stable. Hence, a natural stability criterion can be formulated by decomposing the force  $\mathbf{F}$  onto the non-orthogonal basis  $\{\mathbf{b}_1, \mathbf{b}_2, \mathbf{b}_3\}$  uniquely identified by the structure of the packing (Novak, Samadani & Kudrolli 2005).

### 3.1.1. Change of Basis

Let  $\mathcal{E} = \{\mathbf{e}_1, \mathbf{e}_2, \mathbf{e}_3\}$  be the canonical orthonormal basis of the Euclidean space  $\mathbb{R}^3$  and  $\mathcal{B} = \{\mathbf{b}_1, \mathbf{b}_2, \mathbf{b}_3\}$  a generally non-orthogonal basis with  $\mathbf{b}_\alpha$  unit vectors, and  $\alpha = \{1, 2, 3\}$ . Let  $F_\alpha$  be the components of the maximum force  $\mathbf{F}$  in the canonical basis and  $F'_\alpha$  its components in the basis  $\mathcal{B}$ , i.e.

$$\mathbf{F} = \sum_{\alpha=1}^3 F_\alpha \mathbf{e}_\alpha = \sum_{\alpha=1}^3 F'_\alpha \mathbf{b}_\alpha. \quad (3.2)$$

The components of  $\mathbf{F}$  in the two basis are related through a linear transformation  $\mathbf{A}$ ,

$$(F_1, F_2, F_3) = \mathbf{A}(F'_1, F'_2, F'_3) \quad (3.3)$$

with  $(F_1, F_2, F_3)$  and  $(F'_1, F'_2, F'_3)$  column vectors, and  $\mathbf{A}$  the matrix of direction cosines whose components are defined as  $A_{\alpha\beta} = \cos(\mathbf{b}_\beta, \mathbf{e}_\alpha) = \mathbf{b}_\beta \cdot \mathbf{e}_\alpha$ .

In the  $\mathcal{B}$ -coordinate system and for any sphere belonging to the first mobile layer (i.e.  $n = 1$ ), equation (3.1) simplifies to

$$F'_\alpha = f_b \quad \alpha = \{1, 2, 3\}, \quad (3.4)$$

and the stability criterion is

$$F'_\alpha \leq f_b, \quad \alpha = \{1, 2, 3\}. \quad (3.5)$$

Combining (3.3) and (3.5) yields to

$$B_{\alpha\beta} F_\beta \leq f_b, \quad \alpha, \beta = \{1, 2, 3\}, \quad (3.6)$$

where  $B_{\alpha\beta}$  are the components of  $\mathbf{B} := \mathbf{A}^{-1}$ .

### 3.1.2. Packing orientation

The effect of the packing orientation on the pile stability can be explicitly incorporated. Without loss of generality, let us consider a counterclockwise rotation of the pile (and therefore of the basis  $\mathcal{B}$ ) around the wall-normal, i.e.  $y$ -axis (see Figures 4 (a) and (b)). Such solid-body rotation is fully described by the rotation matrix  $\mathbf{R}_y(\theta)$  defined as

$$\mathbf{R}_y(\theta) = \begin{bmatrix} \cos \theta & 0 & \sin \theta \\ 0 & 1 & 0 \\ -\sin \theta & 0 & \cos \theta \end{bmatrix} \quad (3.7)$$

where  $\theta$  is the rotation angle. The matrix of direction cosines for the rotated system,  $\mathbf{A}_\theta$ , is

$$\mathbf{A}_\theta = \mathbf{R}_y(\theta) \mathbf{A}. \quad (3.8)$$

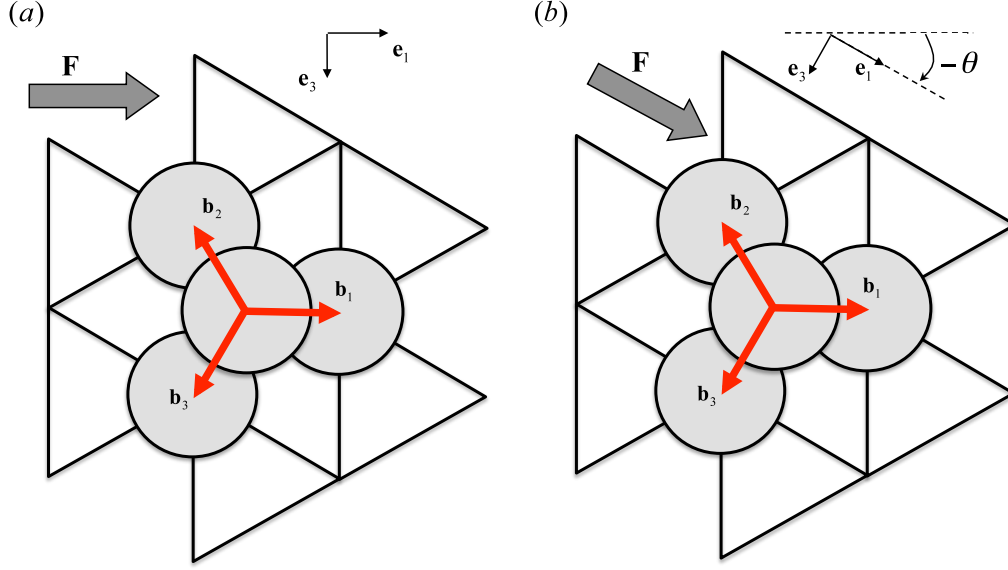


FIGURE 4. Top view of the bottom two layers of a regular isostatic packing of mono-disperse spheres before (a) and after (b) a counterclockwise rotation  $\theta$  of the packing.

The stability criterion (3.5) now implies

$$B_{\theta,\alpha\beta} F_\beta \leq f_b \quad (3.9)$$

where  $B_{\theta,\alpha\beta}$  are the components of  $\mathbf{B}_\theta = (\mathbf{A}_\theta)^{-1}$ .

### 3.1.3. Stability criterion: flow in a fracture

The maximum force  $\mathbf{F}$  is parallel to the fracture walls. Let the axis  $\mathbf{e}_2$  of the cartesian basis  $\mathcal{E}$  be orthogonal to the fracture boundary and  $\mathbf{e}_1$  parallel to  $\mathbf{F}$  such that  $\mathbf{F} = [F, 0, 0]$  where  $F = |\mathbf{F}|$ . We take the projection of  $\mathbf{b}_1$  onto the  $xz$ -plane parallel to  $\mathbf{e}_1$  as a reference configuration for the packing orientation (Fig. 4(a)). Therefore, the components of the basis vectors  $\{\mathbf{b}_1, \mathbf{b}_2, \mathbf{b}_3\}$  in the canonical basis  $\mathcal{E}$  and the matrix of direction cosines  $\mathbf{A}$  are

$$\begin{aligned} \mathbf{b}_1 &= \frac{1}{\epsilon} \begin{bmatrix} \sqrt{3}\ell/3 \\ -h \\ 0 \end{bmatrix}, & \mathbf{b}_2 &= \frac{1}{\epsilon} \begin{bmatrix} -\sqrt{3}\ell/6 \\ -h \\ -\ell/2 \end{bmatrix}, & \mathbf{b}_3 &= \frac{1}{\epsilon} \begin{bmatrix} -\sqrt{3}\ell/6 \\ -h \\ \ell/2 \end{bmatrix}, \\ \mathbf{A} &= \frac{1}{\epsilon} \begin{bmatrix} \sqrt{3}\ell/3 & -\sqrt{3}\ell/6 & -\sqrt{3}\ell/6 \\ -h & -h & -h \\ 0 & -\ell/2 & \ell/2 \end{bmatrix}. \end{aligned} \quad (3.10)$$

The matrix of direction cosines  $\mathbf{A}_\theta$  after a counterclockwise rotation of angle  $\theta$  about  $\mathbf{e}_2$ -axis (Fig. 4 (b)) has the following components

$$\mathbf{A}_\theta = \frac{1}{\epsilon} \begin{bmatrix} (\sqrt{3}\ell/3) \cos \theta & -(\sqrt{3}\ell/6) \cos \theta - (\ell/2) \sin \theta & -(\sqrt{3}\ell/6) \cos \theta + (\ell/2) \sin \theta \\ -h & -h & -h \\ -(\sqrt{3}\ell/3) \sin \theta & (\sqrt{3}\ell/6) \sin \theta - (\ell/2) \cos \theta & (\sqrt{3}\ell/6) \sin \theta + (\ell/2) \cos \theta \end{bmatrix}. \quad (3.11)$$

Therefore, the stability criterion (3.9) is

$$\begin{cases} (2\sqrt{3}/3)(\epsilon/\ell)F \cos \theta < f_b \\ -(2\sqrt{3}/3)(\epsilon/\ell)F \cos(\theta - \pi/3) < f_b \\ -(2\sqrt{3}/3)(\epsilon/\ell)F \cos(\theta + \pi/3) < f_b \end{cases}, \quad (3.12)$$

where  $F$  is the (as yet unknown) total force exerted by the fluid and the pile on the first layer of grains ( $n = 1$ ). In the following section we determine this force.

### 3.2. Shear stress, drag coefficient and maximum load

As discussed in section 2.3,  $\mathbf{F}(n)$  is the drag force exerted by the creeping fluid on a sphere belonging to layer  $n$ . Let  $F'_1(n)$ ,  $F'_2(n)$  and  $F'_3(n)$  be its components along the lattice directions  $\mathbf{b}_1$ ,  $\mathbf{b}_2$ ,  $\mathbf{b}_3$  such that  $\mathbf{F}(n) = F'_1(n)\mathbf{b}_1 + F'_2(n)\mathbf{b}_2 + F'_3(n)\mathbf{b}_3$ . The maximum load is experienced at the bottom of the pile where the total force  $\mathbf{F}$  exerted on the grains of the first layer is

$$\mathbf{F} = \sum_{n=1}^N \mathbf{F}(n) = F'_1\mathbf{b}_1 + F'_2\mathbf{b}_2 + F'_3\mathbf{b}_3, \quad (3.13)$$

where  $F'_\alpha = \sum_{n=1}^N F'_\alpha(n)$ ,  $\alpha = \{1, 2, 3\}$ . While equations (2.21) and (3.13) provide a general framework for the calculation of the maximum force  $\mathbf{F}$  in any regular packings (e.g. hexagonal), in a CEP configuration  $\mathbf{F}$  can be readily calculated from (2.19) by

$$\mathbf{F} = \mathbf{e}_1 \int_0^U \ell M du = \ell MU \mathbf{e}_1, \quad (3.14)$$

where  $U$  is given by (5.3) or (5.5) for laminar or turbulent regime, respectively (see Appendix). The dimensional force is therefore  $\hat{\mathbf{F}} = \mu_e \hat{\ell} \hat{U}$ . When  $\text{Da} \rightarrow 0$ ,  $U \approx \delta \sqrt{\text{Da}/M}$  and

$$|F| \approx \ell \delta \sqrt{M \text{Da}}^{1/2}, \quad (3.15)$$

which provides a scaling for the maximum force in terms of  $\text{Da}$ .

### 3.3. Fluidization Threshold

Combining (3.14) with (3.12), the stability criterion can be written as

$$\begin{cases} 1 - (2\sqrt{3}/3)\text{Ca}^* \cos \theta > 0 \\ 1 + (2\sqrt{3}/3)\text{Ca}^* \cos(\theta - \pi/3) > 0 \\ 1 + (2\sqrt{3}/3)\text{Ca}^* \cos(\theta + \pi/3) > 0 \end{cases} \quad (3.16)$$

where

$$\text{Ca}^* = \frac{\epsilon MU}{f_b}, \quad (3.17)$$

is a capillary number that incorporates geometrical effects of the porous structure. Assuming a toroidal shape of the liquid surface of the capillary bridges, the dimensional capillary force  $\hat{f}_b = \mu q H f_b$  can be related to the dimensional surface tension  $\hat{\gamma} = \mu q \gamma$  and the contact angle between the wetting liquid (e.g. oil) and the surface of the spheres  $\phi$  by

$$\hat{f}_b = 2\pi R \hat{\gamma} \cos \phi \quad (3.18)$$

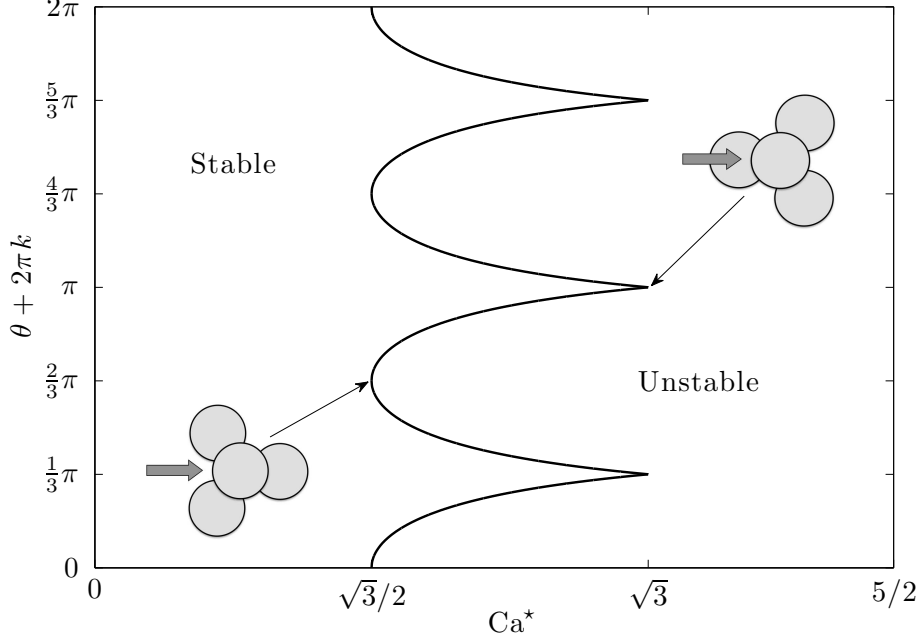


FIGURE 5. Fluidization threshold of a wet granulate under hydrodynamic shear in terms of packing orientation  $\theta$  and capillary number  $\text{Ca}^*$ .

(Scheel *et al.* 2008, p. 190) or, in terms of dimensionless quantities, by  $f_b = \pi\epsilon\gamma \cos \phi$ . Therefore,

$$\text{Ca}^* = \frac{M}{\pi \cos \phi} \text{Ca}, \quad (3.19)$$

where

$$\text{Ca} = \frac{\mu \hat{U}}{\hat{\gamma}}, \quad (3.20)$$

is the capillary number defined in terms of the interfacial coupling velocity  $\hat{U}$ . Solution of (3.16) leads the following stability criterion for the CEP as a function of packing orientation  $\theta$  and capillary number  $\text{Ca}^*$ ,

$$\begin{cases} \text{Ca}^* < \sqrt{3}/2, & \text{stable} & \forall \theta \\ \text{Ca}^* > \sqrt{3}, & \text{unstable} & \forall \theta \\ \sqrt{3}/2 < \text{Ca}^* < \sqrt{3}, & \text{stable for } \theta \in [\arccos(\sqrt{3}/2\text{Ca}^*), 2\pi/3 - \arccos(\sqrt{3}/2\text{Ca}^*)]. \end{cases} \quad (3.21)$$

A graphical representation of (3.21) is provided in Figure 5. The stability of a pile with CEP arrangement of its grains is affected by the orientation of the lattice directions relative to the average velocity of the flow by a factor of 2 (see Figure 5): the pile orientation determines how the destabilizing hydrodynamic forces decompose along the lattice directions and, consequently, how they are balanced by the stabilizing capillary forces acting at the contact points. While the height of the pile does not explicitly affect its stability, the net shearing velocity  $\hat{U}$  is the parameter that controls the fluidization

threshold. For  $\text{Da} \rightarrow 0$ ,  $U \sim \delta\sqrt{\text{Da}/M}$  (Eq. (4.3), Battiato 2011) that, combined with (3.17) and (2.14), leads to

$$\text{Ca}^* = \frac{\delta\epsilon^2}{f_b} \sqrt{Mf(\phi)}. \quad (3.22)$$

Therefore, higher porosity piles are less stable than lower porosity ones, as  $f(\phi)$  is an increasing function of  $\phi$ . This result helps to explain the experimental data of Iverson *et al.* (2000).

#### 4. Summary and Conclusions

By means of a multi-scale framework, we have provided closed-form expressions for the fluidization threshold of a regular packing of mono-disperse frictionless cohesive spherical grains in a planar fracture. The compound effect of structural (e.g. porosity, grain contacts distribution, pile orientation) and dynamical (e.g. capillary and hydrodynamic forces) properties of the system on its stability is taken into account. The impact of packing orientation and porosity is quantified. The orientation of a CEP pile affects its stability threshold by a factor of 2 and an increase in porosity renders a pile more unstable. This helps to explain the high impact of porosity on landslides as experimentally observed by Iverson *et al.* (2000). Moreover, while the height of the pile does not explicitly affect its stability, we identify the capillary number,  $\text{Ca}^*$  (3.17), as the dimensionless parameter that controls the fluidization threshold.  $\text{Ca}^*$  is the ratio between destabilizing hydrodynamic forces (3.14) and stabilizing cohesive (capillary) forces (3.18). It is defined in terms of the net shearing velocity  $\bar{U}$ , the fluid viscosity  $\mu$ , the surface tension  $\hat{\gamma}$ , and the contact angle  $\phi$  between the wetting liquid and the surface of the solid grains. For simplicity, gravity was neglected. We stress that, while applied to cohesive capillary forces, the method can also be used to model any type of cohesive forces (e.g. Van der Waals). The fluidization threshold is then formulated in terms of a dimensionless number defined by the same ratio of forces. Generalisation to include gravity effects is also straightforward.

The impact of i) regular packing structures other than cubic (e.g. arrangements derived from hexagonal close packing), ii) size and density polydispersity, and iii) randomness in grain contacts distribution will be subject of future research.

#### 5. Appendix

Solution of the flow problem (2.10)-(2.13) has been derived in (Battiato, Bandaru & Tartakovsky 2010; Battiato 2011). It is reproduced here for completeness.

##### 5.1. Flow in the granular pile

Velocity distribution inside the granular pile is obtained by integrating the Brinkman equation (2.11) subject to the first and third boundary conditions (2.13)

$$u(y) = \text{Da} + C_1 e^{\lambda y} + C_2 e^{-\lambda y}, \quad y \in [-1, 0], \quad (5.1a)$$

where  $\lambda = 1/\sqrt{M\text{Da}}$  and

$$C_1 = \frac{(U - \text{Da})e^{\lambda} + \text{Da}}{e^{\lambda} - e^{-\lambda}}, \quad C_2 = -\frac{(U - \text{Da})e^{-\lambda} + \text{Da}}{e^{\lambda} - e^{-\lambda}}. \quad (5.1b)$$

The unknown velocity  $U$  at the interface  $y = 0$  between the porous and free flows is determined by matching the flow in the granular pile (5.1) with the free flow. Velocity

profiles for the latter are derived in the following section for laminar and turbulent regimes.

## 5.2. Flow above the granular pile

### 5.2.1. Laminar regime

A solution of the flow equation (2.12) with  $\gamma = 0$  subject to the second and third boundary conditions (2.13) is

$$u(y) = -\frac{y^2}{2} + \left(\delta - \frac{U}{2\delta}\right)y + U, \quad y \in [0, 2\delta]. \quad (5.2)$$

The interfacial velocity  $U$  is obtained from the continuity of the shear stress at  $y = 0$ , the last boundary condition (2.13), as

$$U = \text{Da} \frac{1 - \text{sech} \lambda}{\beta} + \frac{\delta}{\lambda M} \frac{\tanh \lambda}{\beta}, \quad \beta = 1 + \frac{\tanh \lambda}{2\delta \lambda M}. \quad (5.3)$$

The velocity distribution inside the pile is now uniquely defined by combining (5.1) and (5.3). Small Darcy number  $\text{Da}$  corresponds to a plug-flow regime with uniform velocity (i.e. Darcy velocity) almost everywhere in the computational domain; for increasing values of  $\text{Da}$  the velocity profile tends to Poiseuille flow solution (i.e. parabolic profile) as shown in Figure 2 from Battiatto, Bandaru & Tartakovsky (2010), representing the resulting velocity profiles for  $M = 1$ ,  $\epsilon = 0.001$ ,  $\delta = 100$ , and several values of the Darcy number  $\text{Da}$ .

### 5.2.2. Turbulent regime

A number of solutions of (2.12) with  $\gamma = 1$  can be found in chapter 7 of Pope (2000). Assuming the top of the pile to be hydrodynamically smooth, the dimensionless mean velocity  $u$  in the viscous sublayer of dimensionless width  $\delta_\nu$  obeys the *law of the wall* (Pope 2000, pp. 270-271),

$$u(y) = \delta y + U, \quad y \in [0, \delta_\nu]. \quad (5.4)$$

The continuity of the shear stress at  $y = 0$ , i.e., the last boundary condition (2.13), yields an expression for the dimensionless interfacial velocity,

$$U = \text{Da}(1 - \text{sech} \lambda) + \frac{\delta}{\lambda M} \tanh \lambda. \quad (5.5)$$

The comparison of (5.3) and (5.5) reveals that the interfacial velocities  $U$  in the laminar and turbulent regimes differ by the factor  $\beta$ . One can verify that  $\beta \rightarrow 1$  as the Darcy number  $\text{Da} \rightarrow 0$ , i.e. when the permeability and porosity of granular pile become small. For such conditions, equation (5.5) represents a good approximation of (5.3).

## REFERENCES

- ALBERT, R., ALBERT, I., HORNBAKER, D. J., SCHIFFER, P. & BARABÀSI, A.-L. 1997 Maximum angle of stability in wet and dry granular media. *Phys. Rev E* **56**(6), R6271–R6274.
- ALONSO, J. J. & HERRMANN, H. J. 1996 Shape of the tail of a two-dimensional sandpile. *Phys. Rev. Lett.* **76**(26), 4911–4914.
- AURIAULT, J.-L. 2009 On the domain of validity of Brinkman’s equation. *Transp. Porous Med.* **79**, 215–223.
- BAGNOLD, R. A. 1941 *The Physics of Blown Sand and Desert Dunes*. Methuen, London, UK.
- BATTIATO, I. 2011 Universal response of carbon nanotube forests to aerodynamic shear. *J. Fluid Mech.* (under review).

- BATTIATO, I., BANDARU, P. R. & TARTAKOVSKY, D. M. 2010 Elastic response of carbon nanotube forests to aerodynamic stresses. *Phys. Rev. Lett.* **105**(14), 144504.
- DIKAU, R. & BRUNSDEN, D. 1996 *Landslide Recognition: Identification, Movement and Causes*. John Wiley & Sons, London, UK.
- DURAN, J. 2000 *Sands, Powders, and Grains*. Springer-Verlag, New York, USA.
- EBRAHIMNAZHAD-RAHBARI, S. H., VOLLMER, J., HERMINGHAUS, S. & BRINKMANN, M. 2009 A response function perspective on yielding of wet granular matter. *EPL* **87**, 14002.
- FINGERLE, A., ROELLER, K., HUANG, K. & HERMINGHAUS, S. 2008 Phase transitions far from equilibrium in wet granular matter. *New Journal of Physics* **10**, 053020.
- FRAY, K.M. & MARONE, C. 2002 Effect of humidity on granular friction at room temperature. *J. Geophys. Res.* **107**(B11), 2309.
- FRAYSSE, N., THOMÉ, H. & PETIT, L. 1999 Humidity effects on the stability of a sandpile. *Eur. Phys. J. B* **11**, 615–619.
- HANSEN, C.J., BOURKE, M., BRIDGES, N.T., BYRNE, S., COLON, C., DINIEGA, S., DUNDAS, C., HERKENHOFF, K., MCEWEN, A., MELLON, M., PORTYANKINA, G. & THOMAS, N. 2011 Seasonal erosion and restoration of mars' northern polar dunes. *Science* **331**, 575–578.
- HERMINGHAUS, S. 2005 Dynamics of wet granular matter. *Adv. Phys.* **54**(3), 221–261.
- HINCH, E. J. 1977 An averaged-equation approach to particle interactions in a fluid suspension. *J. Fluid Mech.* **83**, 695–720.
- HORNBAKER, D. J., ALBERT, R., ALBERT, I., BARABÀSI, A.-L. & SCHIFFER, P. 1997 What keeps sandcastles standing? *Nature* **387**, 765.
- HOWELLS, I. D. 1974 Drag due to the motion of a newtonian fluid through a sparse random array of small fixed rigid objects. *J. Fluid Mech.* **64**, 449–475.
- IVERSON, R. M. 2000 Landslide triggering by rain infiltration. *Water Resour. Res.* **36**(7), 1897–1910.
- IVERSON, R. M., REID, M. E., IVERSON, N. R., LAHUSEN, R. G., LOGAN, M., MANN, J. E. & BRIEN, D. L. 2000 Acute sensitivity of landslide rates to initial soil porosity. *Science* **290**(5491), 513–516.
- JAEGER, H. M., LIU, C. L. & NAGEL, R. 1989 Relaxation at the angle of repose. *Phys. Rev. Lett.* **62**(1), 40–43.
- JAEGER, H. M., NAGEL, S. R. & BEHRINGER, R. P. 1996 Granular solids, liquids, and gases. *Rev. Mod. Phys.* **68**(4), 1259–1273.
- JOP, P., FORTERRE, Y. & POULIQUEN, O. 2006 A constitutive law for dense granular flows. *Nature* **441**, 727.
- JOP, P., FORTERRE, Y. & POULIQUEN, O. 2007 Initiation of granular surface flows in a narrow channel. *Phys. Fluids* **19**, 088102.
- MASON, T. G., LEVINE, A. J., ERTAS, D. & HALSEY, T. C. 1999 Critical angle of wet sandpiles. *Phys. Rev. E* **60**(5), R5044.
- MIDÍ, GDR 2004 On dense granular flows. *Eur. Phys. J. E* **14**, 341–365.
- MOUKARZEL, C.F. 1998 Isostatic phase transition and instability in stiff granular materials. *Phys. Rev. Lett.* **81**, 1634.
- MOUKARZEL, C.F. 2004 *Carbon nanotubes: science and applications*. The Physics of Granular Media, Wiley-VCH Verlag. 23–43 pp.
- NIEL, D. A., JUNQUEIRA, S. L. M. & LAGE, J. L. 1996 Forced convection in a fluid-saturated porous-medium channel with isothermal or isoflux boundaries. *J. Fluid Mech.* **322**, 201–214.
- NOVAK, S., SAMADANI, A. & KUDROLI, A. 2005 Maximum angle of stability of a wet granular pile. *Nature Phys.* **1**, 50–52.
- POPE, S. B. 2000 *Turbulent Flows*. Cambridge University Press, New York, USA.
- RAJCHENBACH, J. 2003 Dense, rapid flow of inelastic grains under gravity. *Phys. Rev. Lett.* **90**(14), 144302.
- RESTAGNO, F., BOUQUET, L. & CHARLAIX, E. 2004 Where does a cohesive granular heap break? *Eur. Phys. J. E* **14**, 177–183.
- RESTAGNO, F., URSINI, C., GAYVALLET, H. & CHARLAIX, É. 2002 Aging in humid granular media. *Phys. Rev. E* **66**, 021304.

- SCHEEL, M., SEEMANN, R., BRINKMANN, M., MICHIEL, M. DI, SHEPPARD, A., BREIDENBACH, B. & HERMINGHAUS, S. 2008 Morphological clues to wet granular pile stability. *Nat. Mater.* **7**(189), 189–193.
- SCHIFFER, P. 2005 A bridge to sandpile stability. *Nature Phys.* **1**, 21–22.
- TEGZES, P., VICSEK, T. & SCHIFFER, P. 2003 Development of correlations in the dynamics of wet granular avalanches. *Phys. Rev. E* **67**, 051303.
- TORQUATO, S. 2000 *Random Heterogenous Material - Microstructure and Macroscopic Properties*. Springer, New York, USA.
- ULRICH, S., ASPELMEIER, T., ROELLER, K., FINGERLE, A., HERMINGHAUS, S. & ZIPPELIUS, A. 2009 Cooling and aggregation in wet granulates. *Phys. Rev. Lett.* **102**, 148002.
- UMBANHOWAR, P.B., MELO, F. & SWINNEY, H.L. 1996 Localized excitations in a vertically vibrated granular layer. *Nature* **382**, 793–796.
- VAFAI, K. & KIM, S. J. 1990 Fluid mechannics of the interface region between a porous medium and a fluid layer-an exact solution. *Int. J. Heat and Fluid Flow* **11**(3), 254–256.